Meta-analysis of targeted metabolomics data from heterogeneous biological samples provides insights into metabolite dynamics

Ho-Joon Lee[1,2,3,7], Daniel M. Kremer[1,6], Peter Sajjakulnukit[1,6], Li Zhang[1,4], Costas A. Lyssiotis[1,3,5,7]

[1]Department of Molecular and Integrative Physiology, University of Michigan Medical School, Ann Arbor, MI 48109, USA

[2]Michigan Institute for Data Science, University of Michigan, Ann Arbor, MI 48109, USA

[3]Rogel Cancer Center, University of Michigan, Ann Arbor, MI 48109, USA

[4]Michigan Regional Comprehensive Metabolomics Resource Core, University of Michigan, Ann Arbor, MI 48109, USA

[5]Department of Internal Medicine, University of Michigan Medical School, Ann Arbor, MI 48109, USA

[6]Equal contributions

[7]Co-corresponding authors: H.L. (esavant@umich.edu) and C.A.L. (clyssiot@umich.edu)

Abstract

Mass spectrometry-based metabolomics coupled to liquid chromatography, or LC-MS metabolomics, has become the most popular tool for global metabolite abundance profiling to study metabolism. However, the physicochemical complexity of metabolites poses a major challenge for reliable measurements of metabolite abundance. One way to address the issue is to use multiple chromatographic methods to capture a greater range of molecular diversity. We previously developed a tandem mass spectrometry-based label-free targeted metabolomics analysis framework coupled to two distinct chromatographic methods, reversed-phase liquid chromatography (RPLC) and hydrophilic interaction liquid chromatography (HILIC), with dynamic multiple reaction monitoring (dMRM) for simultaneous detection of over 200 metabolites. Our metabolomics framework is designed to study core metabolic pathways and was applied in a wide range of experimental systems including cancer cell lines, tumors, extracellular media, primary cells, immune cells, organoids, organs (e.g. pancreata), tissues, and sera from human and mice. Using 42 heterogeneous deidentified datasets with 635 samples from our platform, we carried out meta-analysis to systematically assess measurement quality in biological replicates and to identify metabolite signatures that reflect biological responses. We show that there exist signature metabolites that correspond to heterogeneous phenotypes, involved in several metabolic pathways. Correlation analysis among our chromatographic methods reveals high confidence metabolites irrespective of experimental systems. We also identify homocystine, reduced glutathione, and phosphoenolpyruvic acid as highly dynamic metabolites across all case-control paired samples. Our study is expected to serve as a reference point for a systematic analysis of label-free LC-MS targeted metabolomics data in both RPLC and HILIC methods with dMRM.

1. Introduction

Cellular metabolism encompasses all the reactions inside a cell that involve small molecules. In order to understand metabolism and its regulation on a global level, metabolomics approaches have become essential for detecting metabolites and measuring their concentrations. Technological advancement of mass spectrometry (MS) has made it a popular and powerful platform for metabolomics studies (Johnson et al., 2016; Patti et al., 2012; Wishart, 2016). Although nuclear magnetic resonance (NMR)-based metabolomics is also widely used, MS is more easily coupled to various chromatographic columns to separate analytes prior to analysis,

thereby reducing the complexity of a biological sample and increasing sensitivity for simultaneous detection of a large number of metabolites (Griffiths et al., 2010; Zhou and Yin, 2016).

Metabolomics can be performed as either targeted or non-targeted. Targeted metabolomics aims to detect and quantify a pre-defined list of specific metabolites, whereas non-targeted or untargeted metabolomics aims to detect and quantify all known and unknown metabolites or compounds in a sample as an unbiased discovery strategy (Dudley et al., 2010; Fuhrer and Zamboni, 2015). Untargeted metabolomics has more challenges than targeted metabolomics, both technically and computationally, and hence its use is more limited than targeted approaches, even in the discovery arena. For example, targeted metabolomics has been used routinely to study well-known metabolic pathways, such as glycolysis, the tricarboxylic acid (TCA) cycle, and nucleotide and amino acid biosynthesis pathways. Nevertheless, detection and quantification of specific metabolites in these pathways can still be challenging, particularly if one aims to target hundreds of metabolites in a single experiment.

MS-based metabolomics is performed predominantly by subjecting samples to chromatographic separation before MS analysis. Chromatographic columns make it possible to separate complex analyte mixtures based on physicochemical properties of a wide range of compounds, including isomers. Liquid chromatography (LC) is most frequently used, while gas chromatography (GC) is preferred for measuring volatile compounds. LC methods include reversed-phase liquid chromatography (RPLC) and hydrophilic interaction liquid chromatography (HILIC). RPLC is typically used for a broad range of metabolites, especially nonpolar and weakly polar metabolites, whereas HILIC has a complementary usage for hydrophilic, polar, and ionic metabolites such as sugars, amino acids, and nucleic acids (Buszewski and Noga, 2012; Cubbon et al., 2010; Ivanisevic et al., 2013; Lu et al., 2008; Rojo et al., 2012; Tang et al., 2016). While a recent study performed a systematic technical evaluation of hydrophilic and hydrophobic LC-MS in metabolomics profiling (Xie et al., 2018), it lacks a biological evaluation of abundance measurements in biological replicates under a wide range of different conditions.

We previously developed a tandem mass spectrometry-based targeted metabolomics system that profiles abundance of more than 200 metabolites as a steady-state snapshot of global metabolism. It utilizes both RPLC and HILIC methods with dynamic MRM (dMRM) as a means to maximize the coverage and sensitivity of target metabolites. Together with our customized computational and statistical analysis pipeline, this platform has been recently applied in several biological contexts (Halbrook et al., 2018; Schofield et al., 2018; Sousa et al., 2016; Svoboda et

al., 2018). Herein, we report heterogeneous data sets from a wide range of experiments and sample types that were generated on our LC-MS/MS targeted metabolomics platform over a period of one year. Using these, we carried out comprehensive global meta-analysis in which we systematically evaluated data quality of both RPLC and HILIC methods by statistical measures and characterized global patterns of metabolite changes and variability in case versus control groups.

2. Materials and methods

2.1. Sample preparation

Preparation of the sample types below has been described before (Halbrook et al., 2018; Schofield et al., 2018; Sousa et al., 2016; Svoboda et al., 2018; Yuan et al., 2012). A brief description follows.

Primary and cultured cells

Biological replicates with n ≥ 3 were seeded at equivalent density, grow in log phase, and at end point media was fully aspirated. Aqueous metabolites of adherent primary or cultured cells on 6-well or 10cm^2 plates were extracted by adding 1 mL or 4 mL of 80% cold (-80°C) methanol, respectively, followed by incubation at -80°C for 10 min. Cells were then scrapped and all material, including soluble and insoluble material, was collected. This was then followed by centrifugation at 14,000 rpm at 4°C for 10 min to pellet the insoluble material. Suspension cells were gently centrifuged to pellet and media was completely aspirated. Metabolites were extracted using the method above. The procedure is done on a bucket of dry ice and as quickly as possible in order to stop metabolism immediately. Samples were normalized by the volume corresponding to protein concentration measured from parallelly prepared lysates (typically, 1 – 2 million cells at 70 – 80% confluence). Then, samples were dried under vacuum and suspended in a 1:1 H_2O/methanol solution for LC-MS analysis.

Tissues, organs, and tumors

Samples of 50 – 200 mg (n ≥ 3) were placed in a tube containing 1 mL of 80% cold (-80°C) methanol and then homogenized using steel beads and a Qiagen Tissue Lyser by multiple rounds of 45-second shaking at room temperature before centrifugation at 14,000 rpm at 4°C for 10 min. Samples were normalized by taking the volume corresponding to 10 mg of the tumor weight and further processed as above for LC-MS analysis.

Cultured media and serum

Metabolites from equivalent volumes of media or serum (n ≥ 3; typically, ~200 µl) were extracted by adding 100% cold (-80°C) methanol with a 1:4 ratio of the sample to methanol (i.e., 80% methanol final) and further processed as above for LC-MS analysis.

2.2. LC-MS metabolomics analysis

Our LC-MS/MS metabolomics analysis was performed as described previously (Halbrook et al., 2018; Schofield et al., 2018; Sousa et al., 2016). In brief, an Agilent 1290 UHPLC and 6490 Triple Quadrupole (QqQ) Mass Spectrometer (LC-MS) were used for label-free targeted metabolomics analysis. Agilent MassHunter Optimizer and Workstation Software LC-MS Data Acquisition for 6400 Series Triple Quadrupole B.08.00 was used for standard optimization and data acquisition. Agilent MassHunter Workstation Software Quantitative Analysis Version B.0700 for QqQ was used for initial raw data analysis.

For RPLC, a Waters Acquity UPLC BEH TSS C18 column (2.1 x 100mm, 1.7µm) was used in the positive ionization mode with mobile phase (A) consisting of 0.5 mM NH_4F and 0.1% formic acid in water; mobile phase (B) consisting of 0.1% formic acid in acetonitrile. Gradient program: mobile phase (B) was held at 1% for 1.5 min, increased to 80% at 15 min, then to 99% at 17 min and held for 2 min before going to initial condition and held for 10 min. For HILIC, a Waters Acquity UPLC BEH amide column (2.1 x 100mm, 1.7µm) was used in the negative ionization mode with mobile phase (A) consisting of 20 mM ammonium acetate (NH_4OAc) in water at pH 9.6; mobile phase (B) consisting of acetonitrile (ACN). Gradient program: mobile phase (B) was held at 85% for 1 min, decreased to 65% at 12 min, then to 40% at 15 min and held for 5 min before going to the initial condition and held for 10 min.

Both columns were at 40℃ and 3 µl of each sample was injected into the LC-MS with a flow rate of 0.2 ml/min. Calibration was achieved through Agilent ESI-Low Concentration Tuning Mix. Optimization was performed on the 6490 QqQ in the RPLC-positive or HILIC-negative mode for each of 245 standard compounds (215 and 217 compounds for RPLC-positive and HILIC-negative, respectively) to obtain the best fragment ion and MS parameters such as fragmentation energy for each standard. Retention time (RT) for each standard was measured from a pure standard solution or a mix standard solution. The LC-MS/MS methods were created with dynamic MRM (dMRM) with RTs, RT windows, and transitions of all 245 standard

compounds (see Supplementary Table). Key parameters of electrospray ionization (ESI) in both the positive and the negative acquisition modes are: Gas temp 275℃, Gas Flow 14 l/min, Nebulizer at 20 psi, SheathGasHeater 250℃, SheathGasFlow 11 l/min, and Capillary 3000 V. For MS: Delta EMV 200V or 350V for the positive or negative acquisition mode respectively and Cycle Time 500ms and Cell Acc 4V for both modes. In this study we denote the dMRM method with RPLC in the positive ionization mode by RPLC-Pos-dMRM and the dMRM method with HILIC in the negative ionization mode by HILIC-Neg-dMRM. We note that our methods do not distinguish stereoisomers, hence care should be taken in interpretation of such data.

2.3. Computational data processing, quality control, and statistical analysis

Pre-processed data with Agilent MassHunter Workstation Software Quantitative Analysis were post-processed for further quality control in the programming language R. First, we examined the distribution of sums of all metabolite abundance peak areas across individual samples in a given experiment as a measure for equal sample loading into the instrument. Any outlier sample was removed, which is defined by a loading difference of greater than 70% compared to the average of the total abundance sums. Next, we calculated coefficients of variation (CVs) in all groups of biological replicate samples ($n \geq 3$) for each metabolite given a cut-off value of peak areas in each of the RPLC-Pos-dMRM and the HILIC-Neg-dMRM methods. We then compared distributions of CVs for the whole dataset for a set of peak area cut-off values of 0, 1000, 5000, 10000, 15000, 20000, 25000 and 30000 in each method. A noise cut-off value of peak areas in each method was chosen by manual inspection of the CV distributions. The noise-filtered data of individual samples were then normalized by the total intensity of all metabolites. We retained only those metabolites with at least 2 replicate measurements for a given experimental variable. The remaining missing value in each condition for each metabolite was filled with the median value of the other replicate measurements. Then, each metabolite abundance level in each sample was divided (i.e., scaled) by the mean of all abundance levels across all samples in a given experiment for comparisons, statistical analyses, and visualizations among metabolites. Finally, we visually inspected a correlation heatmap profile of the samples of the resultant data to identify and remove any further outlier samples based on hierarchical clustering and abnormal heatmap patterns. Pathway analysis was done using the webtool, MetaboAnalyst (Chong et al., 2018).

3. Results and discussion

3.1. Global view of a compendium of heterogeneous targeted metabolomics datasets

We compiled 42 datasets of LC-MS/MS-based targeted metabolomics with both RPLC-Pos-dMRM and HILIC-Neg-dMRM methods. There are a total of 638 samples analyzed, which include cancer cell lines, tumors, extracellular media, primary cells, immune cells, organoids, organs (e.g. pancreata), tissues, sera, and shRNA/drug treatments in human and mice. A total of 448 measurements were made in both methods for 285 unique compound entities (due to multiple detection). We retained measurements for those metabolites detected in both RPLC-Pos-dMRM and HILIC-Neg-dMRM methods as independent measurements. From this compendium we constructed a 448 by 638 data matrix for global characterization. 36.7% of the values in this data matrix were missing, and we removed 11 samples where no compound was measured. Figure 1A depicts a correlation heatmap and a hierarchical clustering of all metabolites in both RPLC-Pos-dMRM and HILIC-Neg-dMRM methods. Figure 1B shows a correlation heatmap and a hierarchical clustering of all samples. We find that there are a few groups of highly correlated metabolites. For example, at the height of 6 in the dendrogram tree, the 31 metabolites in Cluster #1 are enriched in purine, pyrimidine, glycine/serine, and glutathione metabolism, and the 88 metabolites in Cluster #2 include metabolites in the TCA cycle, glycolysis, pyruvate, and phenylalanine/tyrosine/tryptophan metabolism (Figure 1C). This suggests that those metabolites tend to change their abundance in the same direction across different conditions, which suggests that they are subject to pathway level metabolic regulation. The lack of clustering among samples reflects the heterogeneous nature of all datasets and indicates that experimental bias is not driving clustering and influencing downstream analysis. In fact, the most highly correlated 25 samples (Cluster #3, Figure 1B) do not exhibit common phenotypes, and this cluster includes cell lines, murine tumors and several experimentally distinct variables. Therefore, it suggests the existence of general metabolic phenotypes that can arise from various perturbations, independent of cell/tissue type.

3.2. Analysis of normalized relative abundance

Raw data from the LC-MS analysis are peak areas of ion counts for each identified metabolite, which we use as relative abundance values. These raw data do not reflect absolute abundance and cannot be compared directly between experiments run at different times. Accordingly, we examine normalized relative abundance distributions of all metabolites across all datasets using

medians in replicate-group measurements. Figure 2A shows the number of median measurements for each metabolite across all 183 replicate groups. There are a total of 13,026 measurements for 448 metabolites in both RPLC-Pos-dMRM and HILIC-Neg-dMRM methods. 71 metabolites were measured in all 183 replicate groups (Figure 2A). All of these came from the RPLC-Pos-dMRM method. This may indicate that the RPLC-Pos-dMRM method is more robust in detecting those metabolites than the HILIC-Neg-dMRM method. Those most frequently detected metabolites across different conditions are enriched in amino acids, nitrogen, glutathione, and purine metabolism (MetaboAnalyst; FDR < 0.01). The remaining metabolites show a monotonic decrease in the number of measured replicate groups. It is unclear what is the generating function or mechanism of this linearly decreasing distribution.

We next calculated the average of all abundance values for each metabolite. Figure 2B shows a histogram of the average abundance values for all 448 metabolites and Figure 2C shows a distribution of the ordered average abundance values. Three of the top 20 metabolites are involved in cysteine/methionine metabolism (cystine, acetyl-serine, and glutathione) and others in glycolysis, hexosamine, amino acids, mevalonate, energy, and redox metabolism. We also find that one of the top 20 metabolites, phenylalanine, is among the most reproducible metabolites by both RPLC-Pos-dMRM and HILIC-Neg-dMRM methods, along with methionine and taurine, as discussed below (Section 3.4). On the other hand, the bottom 20 metabolites include GDP-glucose, NADP+, fumaric acid, glycerol, dihydrofolate, leucine, docosahexaenoic acid, homocystine, TMP, sucrose, and deoxyadenosine. These metabolites are involved in many different metabolic pathways with no significant enrichment (MetaboAnalyst), suggesting that low abundance is not a pathway-specific or pathway-level feature. Figure 2D is a scatter plot of the average abundance and the number of replicate groups with measurements. The top 5 metabolites are highly abundant in 56 – 183 distinct groups on average, indicating the tendency of more frequent detection of more abundant metabolites. This analysis offers insight into the importance of those relatively high abundant metabolites in diverse conditions with potential effects on phenotypic differences.

3.3. Replicate-group CV analysis of RPLC-Pos-dMRM and HILIC-Neg-dMRM data

The coefficient of variation (CV) is a standard quantitative measure for quality assessment in replicate groups. We calculated biological replicate-group CVs for both the RPLC-Pos-dMRM and HILIC-Neg-dMRM methods and examined their quality differences. Figure 3A shows a

comparison of replicate-group CV distributions of the two methods. There are 28,765 CV values in RPLC-Pos-dMRM and 22,069 CV values in HILIC-Neg-dMRM from all 183 replicate groups for 202 and 195 metabolites, respectively. RPLC-Pos-dMRM measurements show more CVs < 0.2 than HILIC-Neg-dMRM measurements by about two-fold. The summary statistics also show overall better quality of RPLC-Pos-dMRM measurements than HILIC-Neg-dMRM (Figure 3B). This suggests greater chromatographic regularity or compound stability in RPLC-Pos-dMRM than HILIC-Neg-dMRM. To examine the quality in more detail, we restricted our focus to those metabolites with missing values less than 30%. There are 145 such metabolites for RPLC-Pos-dMRM and 77 such metabolites for HILIC-Neg-dMRM. The heatmaps and hierarchical clustering in Figures 3C and 3D show groups of metabolites with low CVs (i.e., better quality; rows in blue) in each method. While we notice overall better quality in RPLC-Pos-dMRM from the heatmaps, there are metabolites with low CVs across all replicate groups in HILIC measurements such as taurine, thymine, phenylalanine, hypotaurine, pyridoxate, methionine, and tryptophan. We also find that amino acids tend to have lower CVs in RPLC-Pos-dMRM than in HILIC-Neg-dMRM, the average CV being 0.25 for RPLC-Pos-dMRM and 0.39 for HILIC-Neg-dMRM.

3.4. Correlation analysis of RPLC-Pos-dMRM and HILIC-Neg-dMRM data

We continued to examine differences between RPLC-Pos-dMRM and HILIC-Neg-dMRM in more detail by focusing on those metabolites that were measured in at least 70% of all 42 experiments with both methods. A total of 3601 measurements were made for 237 metabolites in the 42 experiments. There were 221 metabolites that were measured in at least 2 experiments with both methods. 47 of them were measured in at least 70% of all 42 experiments. For each metabolite in each experiment, we calculated the Pearson correlation coefficient between two abundance profiles measured by the two methods. Figure 4A shows a heatmap of all RPLC-HILIC correlation coefficients, where the metabolites were sorted by the average correlation across all the experiments and the columns were sorted by the average correlation across all the metabolites. Larger circles in darker blues indicate good correlation between the two methods. The top metabolites with reliable measurements across most of the experiments include guanosine, 5-methlythio-adenosine, phosphocreatine, xanthine, proline, taurine, NAD+, and methionine, among others. On the other hand, linoleate, glucuronic acid, 4-hydroxy-L-proline, dehydro-L-ascorbic acid, and acetylcholine, among others show inconsistent

measurements between the two methods, indicating that their retention mechanisms or ionization efficiency may greatly differ between the two methods.

To further examine the 47 metabolites measured by the two methods, we next analyzed abundance CVs in all biological replicate groups. To do this, we first calculated the average of CVs from all replicate groups measured by both methods for each metabolite. Figure 4B shows a distribution of all average CVs, where those metabolites on the left with smaller CVs are more reproducible and hence reliable across the 42 datasets by both methods on average. The top 7 metabolites are methionine, 4-hydroxy-L-proline, phenylalanine, taurine, glutamic acid, hypotaurine, and NAD+ with average CV < 0.3. We also calculated the average of the CVs in each of the two methods. The scatter plot in Figure 4C shows a distribution of the average CVs from the two methods for all 47 metabolites. Given our reference value of CV = 0.4, there are 15 metabolites with CV < 0.4 in both methods that we deem reproducible across diverse conditions. The 3 most reproducible metabolites from both methods are methionine, phenylalanine, and taurine. Phenylalanine was among the top 20 metabolites of high average abundance as discussed above. There are several metabolites which are reliable in either method alone based on the CV = 0.4 cutoff. The RPLC-Pos-dMRM measurements are more reliable for 35 metabolites, whereas the HILIC-Neg-dMRM measurements are more reliable for 17 metabolites.

3.5. Analysis of abundance fold changes for effect size and variability

To study the directionality and magnitude of metabolite changes upon experimental perturbation, we analyzed fold changes (FC) of metabolite abundance across all case-control condition group pairs. For all case-control pairs and each metabolite, we calculated the median ($\tilde{m}$) of normalized abundance values in each group of replicates, i.e., $\tilde{m}_{\text{case}}$ and $\tilde{m}_{\text{control}}$, and the fold change ($\tilde{F}$) of the medians, $\tilde{F} = \tilde{m}_{\text{case}}/\tilde{m}_{\text{control}}$. Then, we calculated the average of absolute values of $log_2(\tilde{F})$ for all case-control pairs for each metabolite, $mean(|log_2(\tilde{F})|)$, which represents an average magnitude of the fold change in the case group relative to the control group for that metabolite. The magnitude or absolute value of $log_2(\tilde{F})$ is also called the effect size.

There are a total of 448 metabolites in 176 case-control pairs from both RPLC-Pos-dMRM and HILIC-Neg-dMRM methods. There are 37.3% missing values in the 448 by 176 data matrix. A missing value occurs when no measurement was made in either a case or control condition. For

a hierarchical clustering of the full data, we removed those metabolites and case-control pairs that have more than 50% missing values across all case-control pairs and all metabolites, respectively. This left us with 294 metabolites and 161 case-control pairs with 15.8% missing values. Figure 5A shows a heatmap of the 294 by 161 data matrix of $log_2(\tilde{F})$ values along with hierarchical clustering dendrograms on both axes. The full 448 by 176 data matrix of fold changes gives us a histogram of all average fold-change magnitudes defined by $mean(|log_2(\tilde{F})|)$ and their ordered distribution in Figure 5B. The average fold-change magnitudes for most metabolites are less than 2 (the peak of the histogram) and the top 20 metabolites with the highest average effect sizes are mostly involved in glycolysis, redox, pyrimidine, and methionine/cysteine/folate metabolism. Homocystine shows the largest average FC magnitude of more than 20, and lactate/glyceraldehyde the second largest of more than 9. We note that lactate and glyceraldehyde were not distinguishable in our HILIC-Neg-dMRM method with identical data. Most of the top 20 metabolites are measured in more than 70 case-control pairs, except homocystine in 9 pairs in the HILIC method and NADP in 12 pairs in the HILIC method (Figure 5C). In addition, we calculated the standard deviation (SD) of the effect sizes for each metabolite to examine the effect-size variability in all case-control pairs for that metabolite. Figure 5D shows a histogram of the SDs and an ordered SD distribution. The SDs for most metabolites are less than 1 and there are 7 metabolites with SD > 3 including lactate/glyceraldehyde and orotate. We also performed an analysis of median absolute deviation (MAD) to complement the SD analysis. Figure 5E shows a MAD histogram and an ordered MAD distribution. The top 20 most variable metabolites with the highest MADs are involved in glycolysis, redox, pyrimidine, energy, and methionine/cysteine/folate metabolism. Figures 5F and 5G show good positive correlations between the average effect sizes and the SD and MAD variability, respectively. Homocystine, lactate/glyceraldehyde, orotate, GSH, and dihydrofolate have both the highest average effect size and the largest variability by both SD and MAD among the top 20, which suggests that they are most dynamic and responsive metabolites across this diverse array of treatments.

4. Conclusion

We performed LC-MS/MS targeted metabolomics to generate 42 datasets in a wide range of experiments and sample types from the same platform in both RPLC-Pos-dMRM and HILIC-Neg-dMRM methods. We carried out a series of computational and statistical analyses to systematically assess data quality of both methods in biological replicate groups to identify more

reliable measurements in each method. We find that the RPLC-Pos-dMRM method tends to generate more reproducible measurements than the HILIC-Neg-dMRM method. Several metabolites are measured reliably in both methods such as methionine, phenylalanine, and taurine. Phenylalanine is among the most abundant metabolites across all samples on average along with acetylcarnitine, cystine, arginine, lactate/glyceraldehyde, UPD-GlcNAc, AMP, GSH, and acetyl-CoA. We also characterized global abundance changes and variability in case-control groups to identify most dynamic and variable metabolites across heterogeneous conditions, such as homocystine, lactate/glyceraldehyde, and GSH. Those metabolites are involved in cysteine metabolism (taurine, cystine, homocystine), glycolysis (glyceraldehyde, lactate), hexosamine biosynthesis (UDP-GlcNAc), redox balance (GSH), fatty acids metabolism (acetylcarnitine, acetyl-CoA), and the TCA cycle (acetyl-CoA). This might suggest that they tend to play more significant roles than others in the associated metabolic pathways under many different conditions. For example, lactate, taurine, methionine, and acetylcarnitine were recently found to be more frequently differentially abundant in tumors compared to normal tissues across different cancer types (Reznik et al., 2018). Our study offers a systematic guideline and a reference point in targeted metabolomics analysis with either RPLC-Pos-dMRM and HILIC-Neg-dMRM method for more reliable biological interpretations.

Data availability

A list of metabolites measured in RPLC-Pos-dMRM and HILIC-Neg-dMRM methods is available in the Supplementary Table along with their formulae, parent mass, product mass, RTs, and CAS numbers. The compendium of randomized and deidentified abundance data is available in the Supplementary Table, which was used in Figures 1A and 1B. The fold-change dataset of case-control condition pairs used in Figure 5 is available in the Supplementary Table after randomization and deidentification of the condition pairs. R codes of all analyses are available upon request.

Acknowledgements

D.M.K is supported by the University of Michigan's Program in Chemical Biology Graduate Assistance in Areas of National Need (GAANN) award. C.A.L. was supported by a Pancreatic Cancer Action Network/AACR Pathway to Leadership award (13-70-25-LYSS); Dale F. Frey

Award for Breakthrough Scientists from the Damon Runyon Cancer Research Foundation (DFS-09-14); Junior Scholar Award from The V Foundation for Cancer Research (V2016-009); Kimmel Scholar Award from the Sidney Kimmel Foundation for Cancer Research (SKF-16-005); a 2017 AACR NextGen Grant for Transformative Cancer Research (17-20-01-LYSS); and UMCCC Core Grant (P30 CA046592). Metabolomics studies performed at the University of Michigan were supported by NIH grant DK097153, the Charles Woodson Research Fund and the UM Pediatric Brain Tumor Initiative.

Author contributions

H.L. conceived the idea, designed the algorithms and pipelines, performed computational and statistical analyses, interpreted the results, and wrote a draft of the manuscript. D.M.K. and P.S. prepared the samples and helped with raw data processing. L.Z. performed LC-MS analysis including raw data generation. D.M.K and L.Z. contributed to writing the manuscript. C.A.L. conceived the idea, interpreted the results, contributed to writing the manuscript, and supervised the project. All authors critically read the manuscript and agreed on the final version.

Conflict of interest

C.A.L. is an inventor on patents pertaining to Kras regulated metabolic pathways, redox control pathways in pancreatic cancer, and targeting GOT1 as a therapeutic approach.

References

Buszewski, B., and Noga, S. (2012). Hydrophilic interaction liquid chromatography (HILIC)--a powerful separation technique. Analytical and bioanalytical chemistry *402*, 231-247.

Chong, J., Soufan, O., Li, C., Caraus, I., Li, S., Bourque, G., Wishart, D.S., and Xia, J. (2018). MetaboAnalyst 4.0: towards more transparent and integrative metabolomics analysis. Nucleic acids research *46*, W486-W494.

Cubbon, S., Antonio, C., Wilson, J., and Thomas-Oates, J. (2010). Metabolomic applications of HILIC-LC-MS. Mass spectrometry reviews *29*, 671-684.

Dudley, E., Yousef, M., Wang, Y., and Griffiths, W.J. (2010). Targeted metabolomics and mass spectrometry. Advances in protein chemistry and structural biology *80*, 45-83.

Fuhrer, T., and Zamboni, N. (2015). High-throughput discovery metabolomics. Current opinion in biotechnology *31*, 73-78.

Griffiths, W.J., Koal, T., Wang, Y., Kohl, M., Enot, D.P., and Deigner, H.P. (2010). Targeted metabolomics for biomarker discovery. Angewandte Chemie (International ed in English) *49*, 5426-5445.

Halbrook, C.J., Pontious, C., Lee, H.-J., Kovalenko, I., Zhang, Y., Lapienyte, L., Dreyer, S., Kremer, D.M., Sajjakulnukit, P., Zhang, L.*, et al.* (2018). Macrophage Released Pyrimidines Inhibit Gemcitabine Therapy in Pancreatic Cancer. bioRxiv, 463125.

Ivanisevic, J., Zhu, Z.J., Plate, L., Tautenhahn, R., Chen, S., O'Brien, P.J., Johnson, C.H., Marletta, M.A., Patti, G.J., and Siuzdak, G. (2013). Toward 'omic scale metabolite profiling: a dual separation-mass spectrometry approach for coverage of lipid and central carbon metabolism. Analytical chemistry *85*, 6876-6884.

Johnson, C.H., Ivanisevic, J., and Siuzdak, G. (2016). Metabolomics: beyond biomarkers and towards mechanisms. Nature reviews Molecular cell biology *17*, 451-459.

Lu, W., Bennett, B.D., and Rabinowitz, J.D. (2008). Analytical strategies for LC-MS-based targeted metabolomics. Journal of chromatography B, Analytical technologies in the biomedical and life sciences *871*, 236-242.

Patti, G.J., Yanes, O., and Siuzdak, G. (2012). Innovation: Metabolomics: the apogee of the omics trilogy. Nature reviews Molecular cell biology *13*, 263-269.

Reznik, E., Luna, A., Aksoy, B.A., Liu, E.M., La, K., Ostrovnaya, I., Creighton, C.J., Hakimi, A.A., and Sander, C. (2018). A Landscape of Metabolic Variation across Tumor Types. Cell systems *6*, 301-313.e303.

Rojo, D., Barbas, C., and Ruperez, F.J. (2012). LC-MS metabolomics of polar compounds. Bioanalysis *4*, 1235-1243.

Schofield, H.K., Zeller, J., Espinoza, C., Halbrook, C.J., Del Vecchio, A., Magnuson, B., Fabo, T., Daylan, A.E.C., Kovalenko, I., Lee, H.J.*, et al.* (2018). Mutant p53R270H drives altered metabolism and increased invasion in pancreatic ductal adenocarcinoma. JCI insight *3*.

Sousa, C.M., Biancur, D.E., Wang, X., Halbrook, C.J., Sherman, M.H., Zhang, L., Kremer, D., Hwang, R.F., Witkiewicz, A.K., Ying, H.*, et al.* (2016). Pancreatic stellate cells support tumour metabolism through autophagic alanine secretion. Nature *536*, 479-483.

Svoboda, L.K., Teh, S.S.K., Sud, S., Kerk, S., Zebolsky, A., Treichel, S., Thomas, D., Halbrook, C.J., Lee, H.J., Kremer, D.*, et al.* (2018). Menin regulates the serine biosynthetic pathway in Ewing sarcoma. The Journal of pathology *245*, 324-336.

Tang, D.Q., Zou, L., Yin, X.X., and Ong, C.N. (2016). HILIC-MS for metabolomics: An attractive and complementary approach to RPLC-MS. Mass spectrometry reviews *35*, 574-600.

Wishart, D.S. (2016). Emerging applications of metabolomics in drug discovery and precision medicine. Nature reviews Drug discovery *15*, 473-484.

Xie, B., Wang, Y., Jones, D.R., Dey, K.K., Wang, X., Li, Y., Cho, J.H., Shaw, T.I., Tan, H., and Peng, J. (2018). Isotope Labeling-Assisted Evaluation of Hydrophilic and Hydrophobic Liquid Chromatograph-Mass Spectrometry for Metabolomics Profiling. Analytical chemistry *90*, 8538-8545.

Yuan, M., Breitkopf, S.B., Yang, X., and Asara, J.M. (2012). A positive/negative ion-switching, targeted mass spectrometry-based metabolomics platform for bodily fluids, cells, and fresh and fixed tissue. Nature protocols *7*, 872-881.

Zhou, J., and Yin, Y. (2016). Strategies for large-scale targeted metabolomics quantification by liquid chromatography-mass spectrometry. The Analyst *141*, 6362-6373.

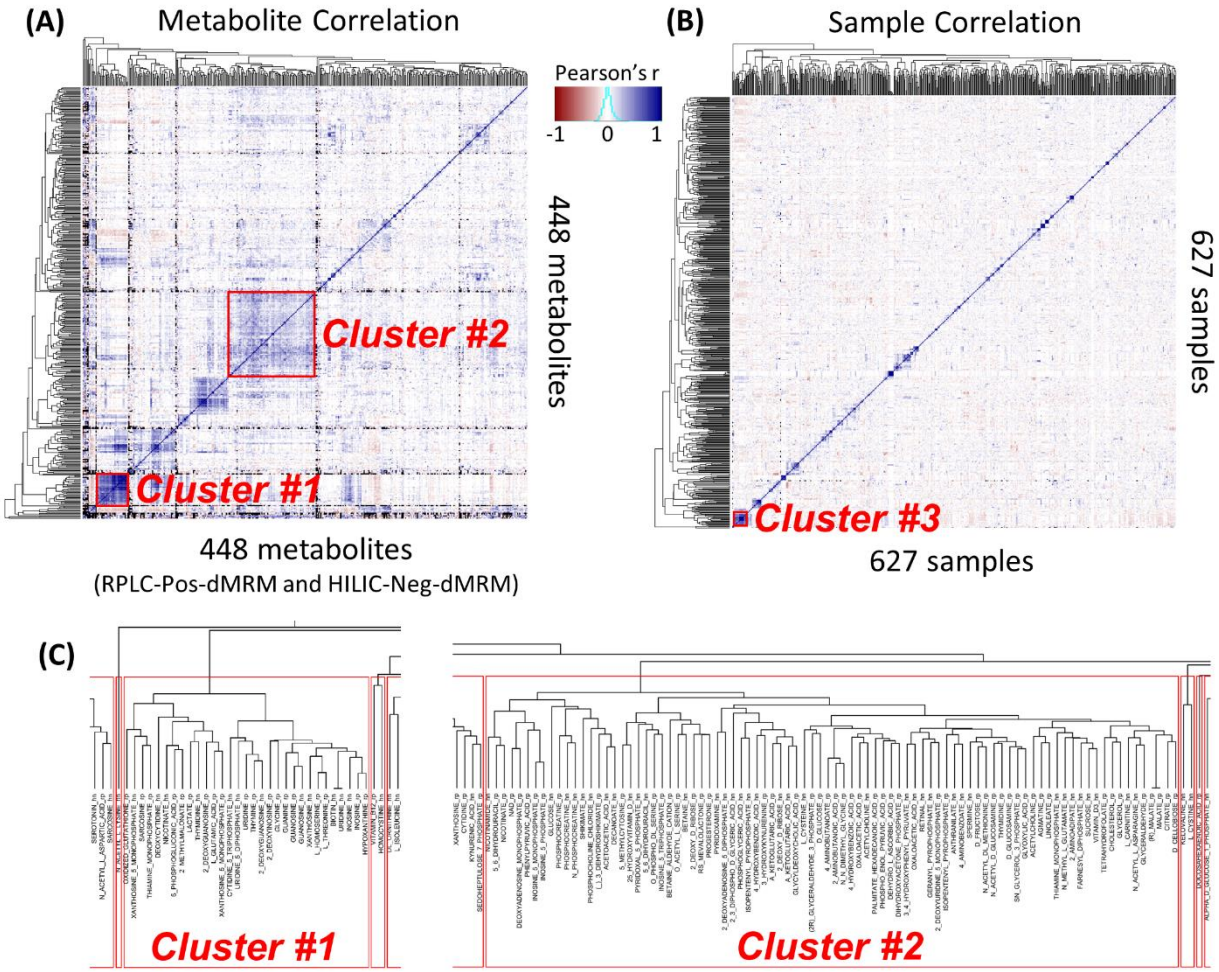

FIGURE 1. Global view of the metabolomics data compendium.

(A) A correlation heatmap of 448 metabolite measurements of relative normalized abundance from both RPLC-Pos-dMRM and HILIC-Neg-dMRM methods along with unsupervised hierarchical clustering. The color key is based on Pearson correlation coefficients. (B) A correlation heatmap of 627 samples along with unsupervised hierarchical clustering. The color code is the same as in (A). See the Supplementary Table for the data used for (A) and (B). (C) Dendrogram trees of Cluster #1 and Cluster #2 at the height of 6. The suffix, "rp", in the metabolite names stands for RPLC-Pos-dMRM and "hn" for HILIC-Neg-dMRM.

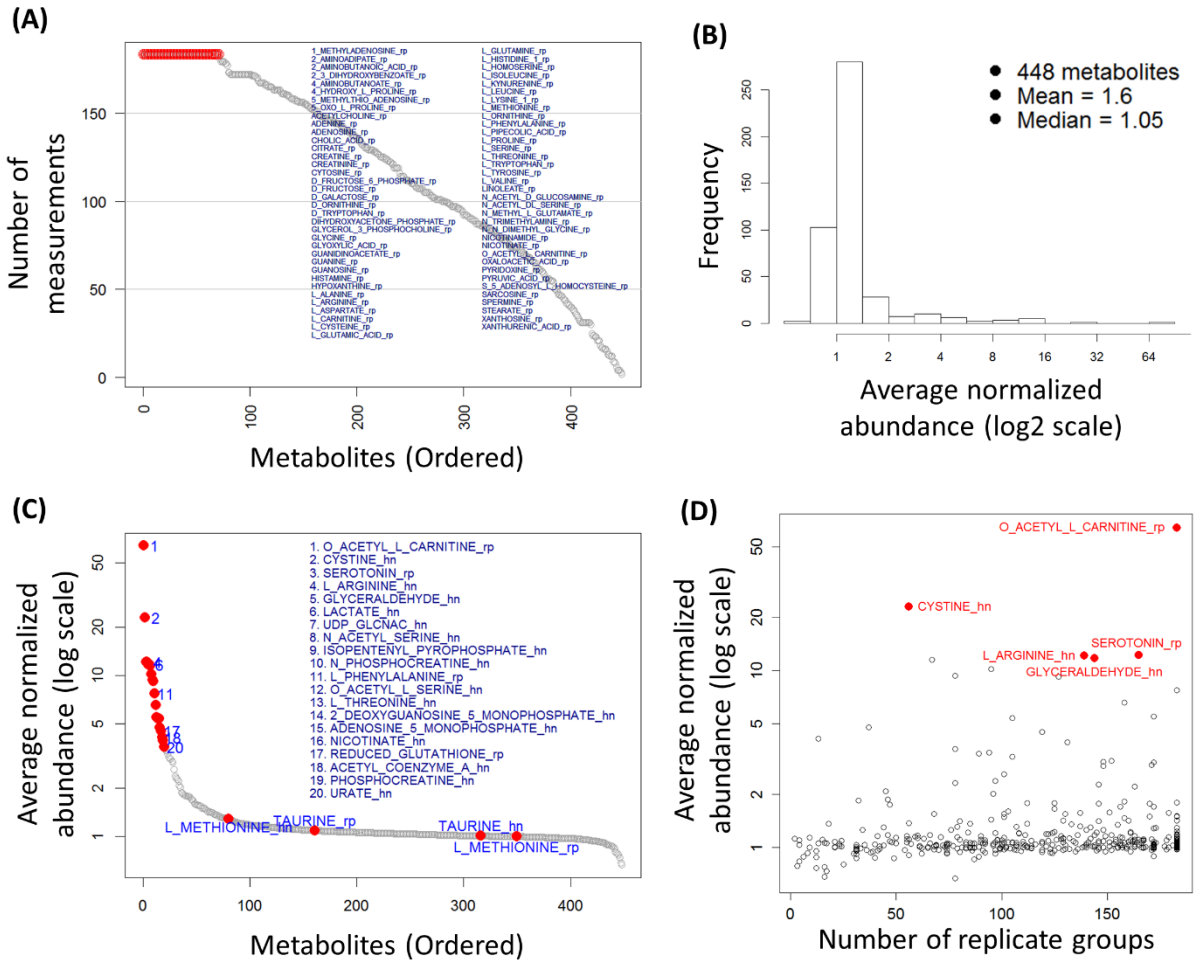

FIGURE 2. Analysis of relative abundance.

(A) The distribution of the numbers of median measurements for 448 metabolites across all 183 biological replicate groups. There are 71 metabolites with measurements in the maximum 183 replicate groups as listed. See also the Supplementary Table for the list of 71 metabolites. (B) A histogram distribution of the average normalized abundance values for all 448 metabolites. (C) An ordered distribution of (B). The top 20 metabolites are listed along with methionine and taurine (cf. Figure 4F). See also the Supplementary Table for the list of the top 20 metabolites. (D) A scatter plot of the average normalized abundance of (B) or (C) and the numbers of replicate groups with measurements. The top 5 highly abundant metabolites are shown in red.

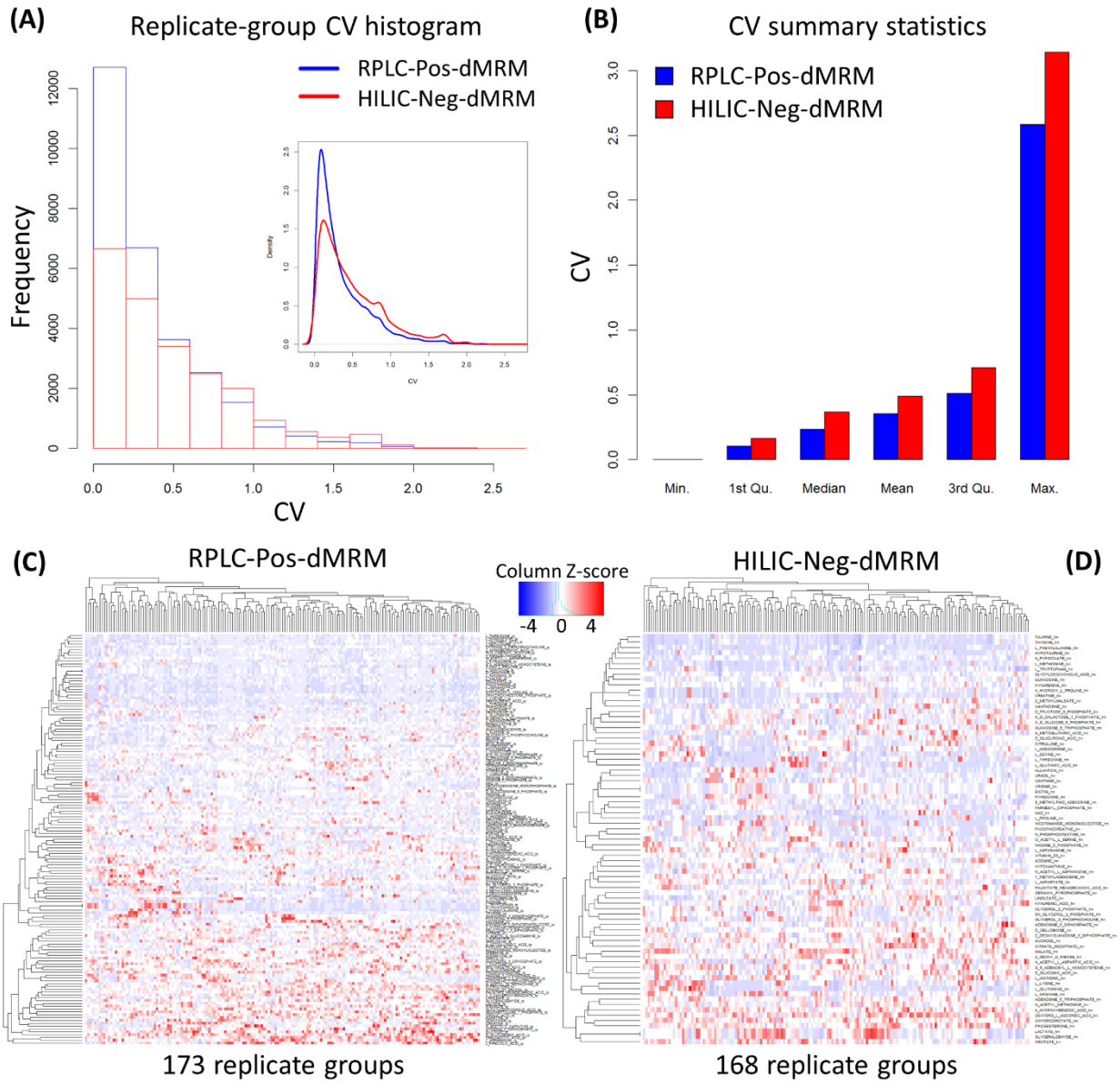

FIGURE 3. Replicate-group CV analysis.

(A) Distributions of replicate-group CVs of the RPLC-Pos-dMRM and HILIC-Neg-dMRM methods. There are 28,765 CV values in RPLC-Pos-dMRM and 22,069 CV values in HILIC-Neg-dMRM from all 183 replicate groups for 202 and 195 metabolites, respectively. (B) Summary statistics of all replicate-group CVs from the two methods. (C) Heatmap and hierarchical clustering of replicate-group CVs for 145 metabolites with missing values less than 30% across all replicate groups in the RPLC-Pos-dMRM method. (D) Heatmap and hierarchical clustering of replicate-group CVs for 77 metabolites with missing values less than 30% across

all replicate groups in the HILIC-Neg-dMRM method. CVs are standardized by the column Z-score in (C) and (D). See also the Supplementary Table for the ordered list of the 145 and 77 metabolites of (C) and (D).

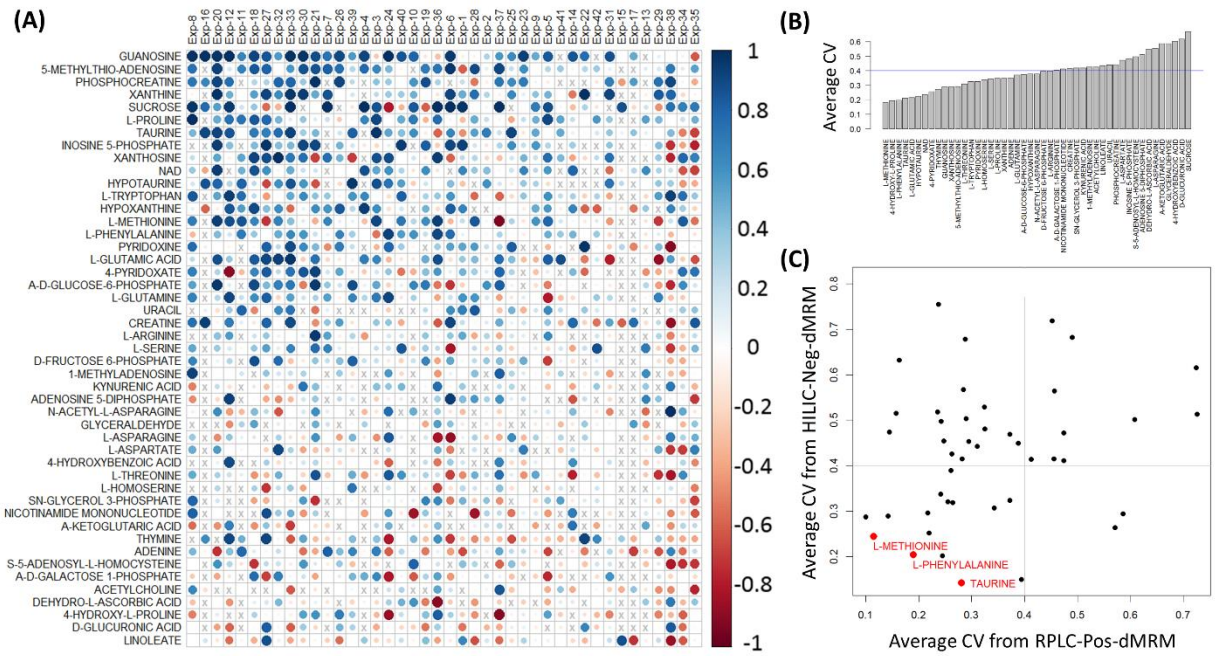

FIGURE 4. RPLC-HILIC correlation analysis.

(A) Heatmap of all RPLC-HILIC Pearson correlation coefficients for 47 metabolites that were measured in at least 70% of all 42 experiments. The metabolites were sorted by the average correlation across all the experiments and the columns were sorted by the average correlation across all the metabolites. Larger circles in darker blues indicate good correlation between the RPLC-Pos-dMRM and HILIC-Neg-dMRM measurements. (B) Distribution of all average CVs across the 42 datasets in both RPLC-Pos-dMRM and HILIC-Neg-dMRM methods. (C) A scatter plot of the average CVs from the RPLC-Pos-dMRM and HILIC-Neg-dMRM measurements for all 47 metabolites. The 3 most reproducible metabolites by both methods are shown in red. See also the Supplementary Table for the list of 47 metabolites along with CV values in both methods.

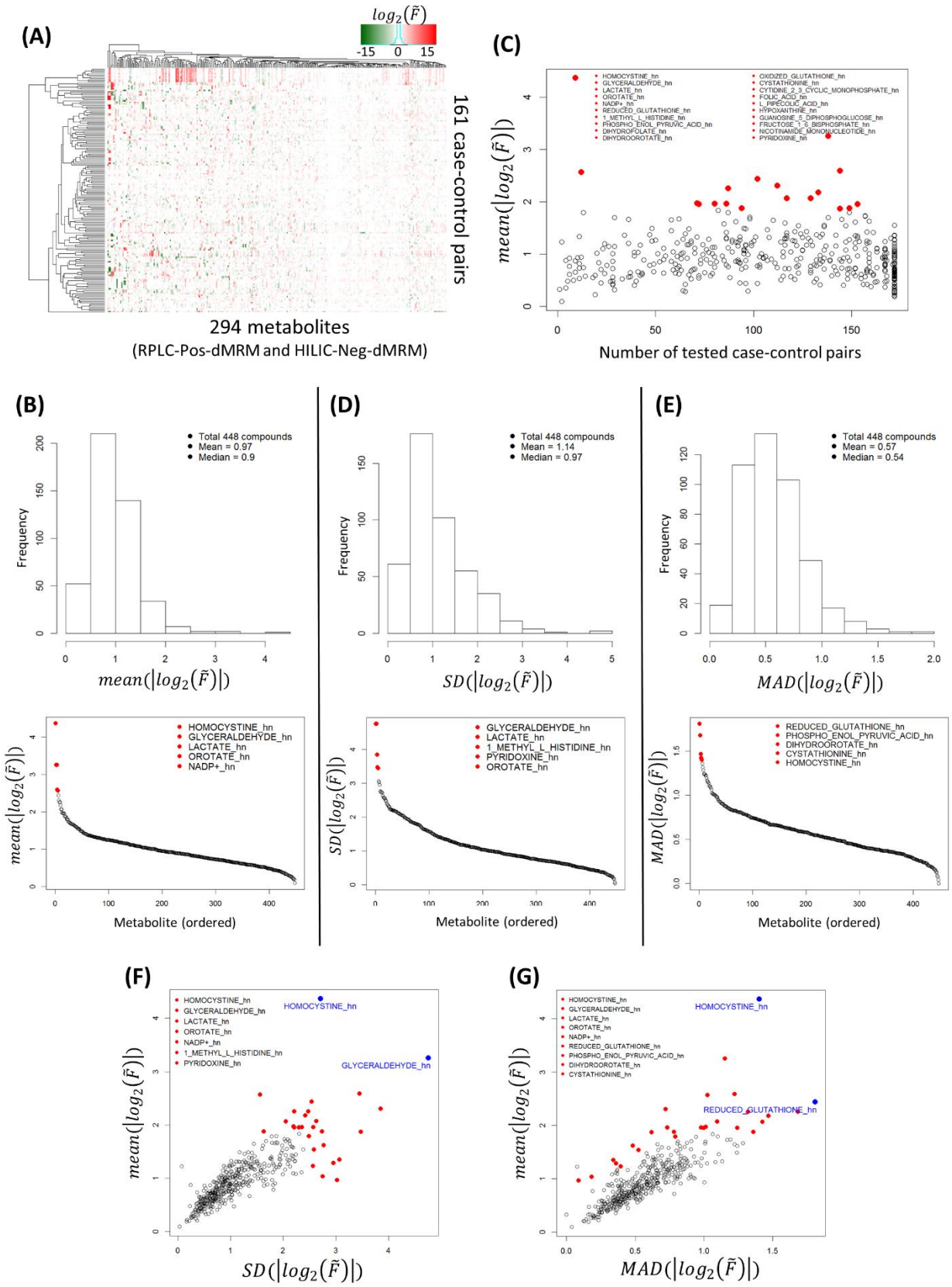
(A)
$log_2(\tilde{F})$
-15 0 15
161 case-control pairs
294 metabolites
(RPLC-Pos-dMRM and HILIC-Neg-dMRM)
(C)
HOMOCYSTINE_hn
GLYCERALDEHYDE_hn
LACTATE_hn
OROTATE_hn
NADP+_hn
REDUCED_GLUTATHIONE_hn
1_METHYL_L_HISTIDINE_hn
PHOSPHO_ENOL_PYRUVIC_ACID_hn
DIHYDROFOLATE_hn
DIHYDROOROTATE_hn
OXIDIZED_GLUTATHIONE_hn
CYSTATHIONINE_hn
CYTIDINE_2_3_CYCLIC_MONOPHOSPHATE_hn
FOLIC_ACID_hn
L_PIPECOLIC_ACID_hn
HYPOXANTHINE_hn
GUANOSINE_5_DIPHOSPHOGLUCOSE_hn
FRUCTOSE_1_5_BISPHOSPHATE_hn
NICOTINAMIDE_MONONUCLEOTIDE_hn
PYRIDOXINE_hn
$mean(|log_2(\tilde{F})|)$
Number of tested case-control pairs
(B)
Total 448 compounds
Mean = 0.97
Median = 0.9
Frequency
$mean(|log_2(\tilde{F})|)$
HOMOCYSTINE_hn
GLYCERALDEHYDE_hn
LACTATE_hn
OROTATE_hn
NADP+_hn
Metabolite (ordered)
(D)
Total 448 compounds
Mean = 1.14
Median = 0.97
Frequency
$SD(|log_2(\tilde{F})|)$
GLYCERALDEHYDE_hn
LACTATE_hn
1_METHYL_L_HISTIDINE_hn
PYRIDOXINE_hn
OROTATE_hn
Metabolite (ordered)
(E)
Total 448 compounds
Mean = 0.57
Median = 0.54
Frequency
$MAD(|log_2(\tilde{F})|)$
REDUCED_GLUTATHIONE_hn
PHOSPHO_ENOL_PYRUVIC_ACID_hn
DIHYDROOROTATE_hn
CYSTATHIONINE_hn
HOMOCYSTINE_hn
Metabolite (ordered)
(F)
HOMOCYSTINE_hn
GLYCERALDEHYDE_hn
LACTATE_hn
OROTATE_hn
NADP+_hn
1_METHYL_L_HISTIDINE_hn
PYRIDOXINE_hn
HOMOCYSTINE_hn
GLYCERALDEHYDE_hn
$mean(|log_2(\tilde{F})|)$
$SD(|log_2(\tilde{F})|)$
(G)
HOMOCYSTINE_hn
GLYCERALDEHYDE_hn
LACTATE_hn
OROTATE_hn
NADP+_hn
REDUCED_GLUTATHIONE_hn
PHOSPHO_ENOL_PYRUVIC_ACID_hn
DIHYDROOROTATE_hn
CYSTATHIONINE_hn
HOMOCYSTINE_hn
REDUCED_GLUTATHIONE_hn
$mean(|log_2(\tilde{F})|)$
$MAD(|log_2(\tilde{F})|)$

FIGURE 5. Abundance fold change analysis.

(A) Heatmap of $log_2(\tilde{F})$ for 294 metabolites and 161 case-control sample pairs. (B) A histogram of all average fold-change magnitudes (= $mean(|log_2(\tilde{F})|)$; effect size) and an ordered distribution of the average magnitudes. The top 20 metabolites are listed. (C) A scatter plot of the average fold-change magnitudes and the numbers of tested case-control pairs. (D) Effect-size variability in terms of the standard deviation (SD). A histogram of SDs of the effect sizes and an ordered SD distribution. The top 5 metabolites are listed. (E) Effect-size variability in terms of the maximum absolute deviation (MAD). A histogram of MADs of the effect sizes and an ordered MAD distribution. The top 5 metabolites are listed. (F) A scatter plot of the average effect sizes and the SD variability. The union of the top 5 metabolites from (B) and (D) are listed. (G) A scatter plot of the average effect sizes and the MAD variability. The union of the top 5 metabolites from (B) and (E) are listed. See the Supplementary Table for the full fold-change dataset.